Journal of Thermal Analysis and Calorimetry (2023) 148:9909–9917
https://doi.org/10.1007/s10973-023-12354-3

Thermal properties investigation of paraffin wax/titania nanocomposites as phase change materials

Shehab A. Mansour[1,2] · Ahmed A. Atwa[1,2] · Elsayed M. Farag[2] · Ragab A. Elsad[1,2]

Received: 22 November 2022 / Accepted: 1 July 2023 / Published online: 7 August 2023
© The Author(s) 2023

Abstract

The use of phase change materials (PCMs) for thermal storage, thermal management, and thermal insulation has been widespread for many years. Thermal storage systems (TES) based on PCMs can be improved and optimized by adding nanoparticles (NPs) to them. Throughout this study, PCM nanocomposites (NCs) based on paraffin wax (PW) loaded by anatase titania (TiO_2) NPs were fabricated and characterized to examine their thermal performance as phase change materials. The as-synthesized TiO_2 NPs were obtained by hydrolysis technique and showed a well-defined spherical shape with a diameter in the nanoscale range and a crystallite size ~ 22.75 nm. Throughout the used concentrations of TiO_2 NPs, 0, 0.05, 0.1, 0.15, 0.2, 0.25, 0.3, and 0.5%, the morphological feature for the PW/TiO_2 NCs revealed a good dispersion of NPs in PW. The non-isothermal differential scanning calorimetry (DSC) measurements at a constant heating rate of 10 °C min^{-1} were used in order to get the melting point (T_m), latent heat of fusion (LH), and latent heat rate (LHR) as a function of TiO_2 NP concentrations for the investigated PW/TiO_2 NCs. Both LH and LHR values for PW/TiO_2 NCs are higher than those obtained for a pure PW sample. The significant enhancement in LH and LHR values for PW/TiO_2 NCs was found to be 21.2% and 134.3% in comparison with the pure PW sample, respectively. The thermal stability of the investigated PW/TiO_2 NCs was examined using thermal gravimetric (TG) scans. It is found that the thermal stability varies with TiO_2 NP concentrations with a non-monotonic trend. At concentrations up to 0.25 mass%, the thermal stability improved. For concentrations over 0.25 mass%, the degradation process became rapid.

Keywords Phase change materials · Paraffin wax · Anatase · TiO_2 · Latent heat · Thermal stability

Abbreviations

EtOH	Ethanol
FE-SEM	Field-emission scanning electron microscope
DSC	Differential scanning calorimetry
DTG	Derivative thermogravimetric
LH	Latent heat
FWHM	Full width at half maximum
NCs	Nanocomposites
NPs	Nanoparticles
PCMs	Phase change materials
PW	Paraffin wax
RT	Room temperature
SH	Sensible heat
LHR	Latent heat rate
TES	Thermal energy storage
TG	Thermogravimetric
TiO_2	Titania
TTIP	Titanium (IV) isopropoxide
XRD	X-ray diffraction

List of symbols

β	Full width at half maximum in radians
θ	The diffraction angle
K	The shape factor
ε	The induced strain in crystal lattice
T_m	Melting temperature
D	Crystallite size
$T_{5\%}$	The temperature at which 5% of the degradation happens
$T_{50\%}$	The temperature at which 50% of the degradation happens

✉ Shehab A. Mansour
shehab_mansour@yahoo.com

[1] Advanced Materials/Solar Energy and Environmental Sustainability (AMSEES) Laboratory, Faculty of Engineering, Menoufia University, Shebin El-kom 32511, Egypt

[2] Basic Engineering Science Department, Faculty of Engineering, Menoufia University, Shebin El-kom, Egypt

T_f The final temperature at which the degradation process ends

T_p Peak temperature at the maximum rate of the degradation process

Introduction

Recently, the significant demand for renewable sources of energy has become urgent, especially with the repeated energy crisis. Thermal energy storage (TES) systems are considered one of the most sustainable and efficient tools for solar energy usage. The utilizing of phase change materials (PCMs) as functional materials in TES systems has significant interest of researchers for their sensible heat (SH) and latent heat (LH). In fact, PCMs can be classified as solid–solid, solid–liquid, solid–gas, and liquid–gas PCMs according to the phases that precede and follow the phase transition. The growing utilization of solid–liquid PCMs is due to their unique thermodynamic properties, such as melting temperature (T_m) in the operating range, suitable LH of melting for the required usage, high thermal stability, and durability [1]. Such properties of PCMs enable TES to be more efficient by reducing the gap between energy supply and demand through the high performance of energy distribution networks. Specific thermal requirements, which primarily rely on the purpose for which it will be used, must be met when choosing a PCM. High LH capacity, T_m appropriate for application temperature levels, non-segregating behavior, low subcooling effect, and small volume variations during the phase transition process are additional physical requirements. Moreover, PCMs should maintain their chemical stability during charging and discharging cycles [2].

The three main subcategories of solid–liquid PCMs are eutectic, inorganic, and organic PCMs. Among the inorganic solid–liquid PCMs are metals, alloys, molten salts, and salt hydrates. For organic solid–liquid PCMs, see parafns, fatty acids, polyethylene glycol, polyalcohol, etc. Also known as composite solid–liquid PCMs, eutectic solid–liquid PCMs are a combination of organic/organic, organic/inorganic, and inorganic/inorganic solid–liquid PCMs [3]. One of the most important organic PCMs is paraffin wax (PW), which is widely used in solar energy storage applications. PW consists mainly of a straight chain of hydrocarbons; it has many advantages for being used as a PCM, such as being chemically and thermally stable at the operating temperatures for most heating applications. The usage of PW as a thermal storage medium enabled numerous advantages by comparing with the conventional heat storage system [4]. Namely, such advantages include the reducing the size and mass of TES besides decreasing the maximum operating temperature that the system reaches. Despite that, PW as an organic PCM has low thermal conductivity and lower melting heat in comparison with inorganic PCMs [5]. In order to overcome this shortcoming, a lot of research works have been done on enhancing the thermal conductivity of PW by introducing inorganic nanoparticles (NPs) such as Al_2O_3, TiO_2, ZnO, CuO, and MWCNTs NPs [6–11]. The introduction of these NPs into PW offers not only enhancements in heat transfer and heat capacity but also increases the thermal stability and durability of PW [12, 13]. Despite this, it is difficult to evenly distribute nanoparticles in PCM and keep them from aggregating, which has limited the use of these materials in research and industry. The stability of nanoparticles in PCM can be increased utilizing a variety of techniques, including the use of surfactants, functionalization of nanoparticles, ultrasonication, and homogenization [14].

Until now, the optimization and understanding of the behavior of PW nanocomposites (NCs) as thermal storage mediums have faced some challenges. Among these is the suitable range of NPs' loading that is enabled by enhancing the thermal properties of PW. Obliviously, the optimum loading concentration of NPs into PCMs depends on various effective factors for the used NPs such as their shape, size, thermal properties, and method of introduction into PCMs. So, there is significant demand for research works to reach the optimum conditions of using PW NCs to be qualified in TES applications. Numerous experiments have been conducted to create high thermal conductivity latent heat TES systems with improved thermal performance by distributing TiO_2 NPs into PW. Despite the fact that the majority of these research focus on relatively high mass percentage ratios of TiO_2 NPs, such as 0.5–2 mass% [15], 1–5 mass% [16], 1–3 mass% [17], and 1–7 mass% [18]. Up to our knowledge, there are no studies in the literatures for the performance of PW/titania with a small range of TiO_2 concentrations. As a result, the current work includes the investigation of the thermal properties of PW/titania (TiO_2) NCs in the low range of TiO_2 NPs concentrations up to 0.5 mass% with different steps of concentration, namely 0, 0.05, 0.1, 0.15, 0.2, 0.25, 0.3 and 0.5 mass%. Such a little amount of TiO_2 addition to PW could enhance nanoparticle Brownian motion, which would improve PW's heat transfer capabilities [19]. The titania NPs that formed were in the anatase phase structure. The phase structure of titania, anatase, is believed to be more stable than rutile, especially at small particle sizes [20]. Additionally, anatase-TiO_2-based nanofluid has been shown to have better thermal conductivity than anatase and rutile mixture-based nanofluid [21]. This result is supported by Mitra et al. [22] using density functional theory on the thermal transport properties of the rutile and anatase TiO_2. The effect of the addition of the synthesized TiO_2 NPs on the thermal properties of PW was studied using non-isothermal techniques: differential scanning calorimetry (DSC) and thermogravimetric (TG) analysis. The characteristic parameters of the melting process were studied using DSC

measurements for the investigated PW TiO_2 NCs. However, the thermal stability was studied using the TG analysis of the investigated NCs.

Experimental

Materials

Ethanol (EtOH) absolute anhydrous (C_2H_5OH from CARLO ERBA Reagents S.A.S), titanium (IV) isopropoxide (TTIP) ($TiC_{12}H_{28}O_{14}$ 97.0% from Aldrich) and a commercial paraffin wax (PW) in pellet shape provided from the Egyptian ELNILE company were used for the preparation of PW/TiO_2 NCs.

Synthesization of TiO_2 nanoparticles

The synthesized TiO_2 NPs were obtained by hydrolysis of TTIP in the presence of EtOH. The method of synthesis used has been described elsewhere [23, 24]. In the typical method, a solution of ethanol and distilled water was made by adding 97 mL of EtOH to 3 mL of distilled water. After that, 3.7 mL of TTIP was gradually added to the solution. At room temperature (RT), the mixture was stirred for 1 h using the magnetic stirrer and then left for 36 h for aging. After that, the obtained solution was introduced into an alumina crucible and placed in an oven for 8 h at 100 °C to obtain a fine white powder. Thereafter, the final fine nanoparticle sample was obtained after an annealing process at 500 °C for 1 h. The selected annealing conditions were used to ensure the formation of TiO_2 in the anatase phase [23]. Figure 1a illustrates the detailed schematic diagram procedure for the synthesization process of TiO_2 NPs.

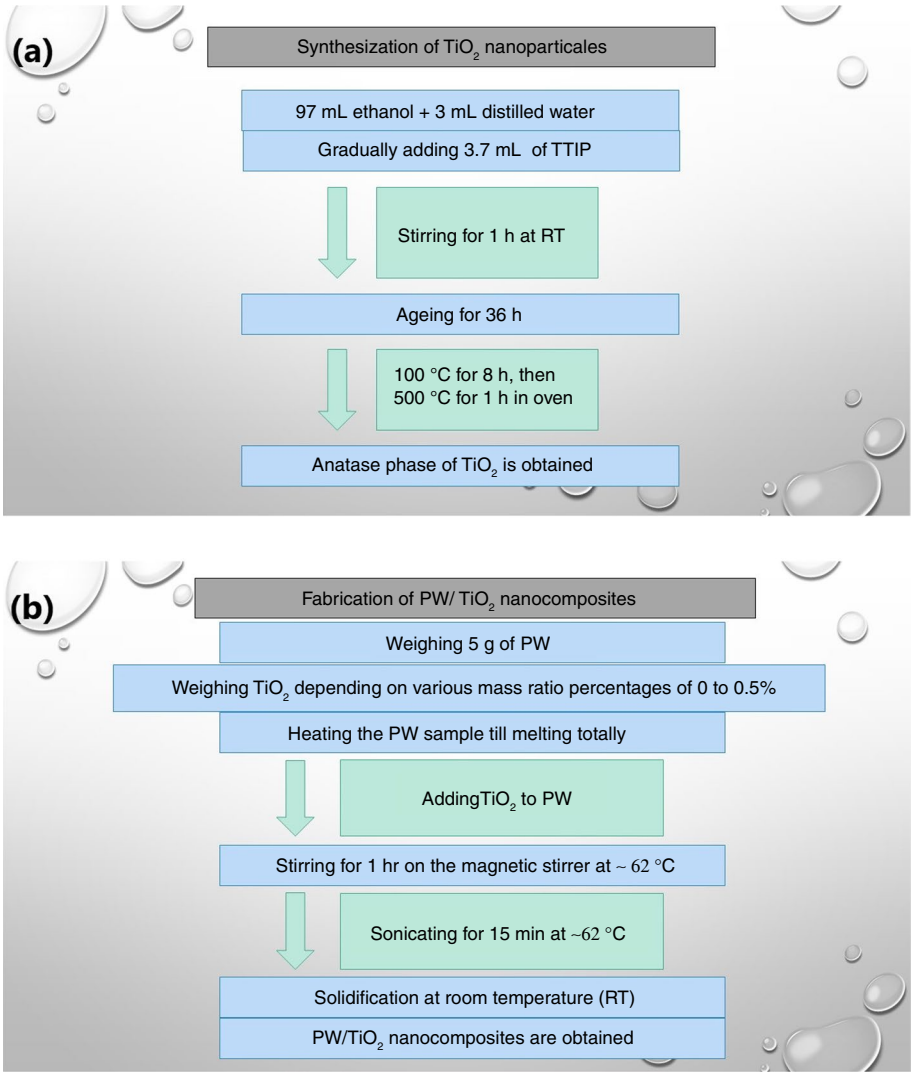

Fig. 1 **a** The schematic diagram for the synthesization process of TiO_2 NPs; **b** the schematic diagram for the fabrication process of PW/TiO_2 NCs

Fabrication of PW/TiO_2 nanocomposites

PW/TiO_2 NCs were fabricated by mixing the synthesized TiO_2 NPs with melted PW. In this respect, 5 g of PW was weighed for each sample and then heated till it was totally melted, and the desired amount of TiO_2 NPs was added to the melted PW while it was on the magnetic stirrer with various mass ratio percentages of 0, 0.05, 0.1, 0.15, 0.2, 0.25, 0.3 and 0.5%. The stirring process was kept for 1 h with the temperature around 62 °C. In order to get good dispersion of the NPs, the mixture of each sample was exposed to ultrasonic radiation around at 62 °C for 15 min using a high power ultrasonic homogenizer, model UP 400 s. Then the NC samples were kept at RT to solidify. The fabricated NC samples were labeled as P, P/0.05T, P/0.1T, P/0.15T, P/0.2T, P/0.25T, P/0.3T and P/0.5T, which corresponds to the used mass ratio percentages between PW and synthesized TiO_2 NPs: 0, 0.05, 0.1, 0.15, 0.2, 0.25, 0.3, and 0.5%, respectively. Figure 1b shows the fabrication process for the investigated PW/TiO_2 NCs. The used mass ratio percentages and the corresponding sample names are illustrated in Table 1

Characterizations and measurements

X-ray diffraction (XRD) was used to examine the crystal structure of the synthesized TiO_2 NPs by using the PANalytical X'Pert PRO MRD X-ray diffractometer with CuKα as a radiation source of wavelength ($\lambda = 0.15406$ nm) at 1800 W power (45 kV, 40 mA). The used diffraction angle (2θ) during the measurement in the range from 10° to 80° with a 0.02°-step field-emission scanning electron microscope (FE-SEM, Quanta FEJ20) was used to check the morphology of the synthesized TiO_2 NPs as well as the fabricated PW/TiO_2 NCs. DSC measurements were used to determine some of the characteristic thermal quantities, such as T_m and LH of fusion for the investigated PW/TiO_2 NCs. In this respect, the SETARAM DSC131 Evo instrument was used for DSC measurements. The nanocomposite sample with a mass ~ 10 mg was introduced into the aluminum crucible. DSC measurements were performed at a constant heating rate of 10 °C min^{-1} and in a temperature range starting from RT to 160 °C. A dynamic nitrogen (N_2) atmosphere with an automatically adjusted flow rate was used during the DSC measurements. In order to study the thermal stability of the investigated NCs, non-isothermal TG measurements were performed using the SETARAM THEMYS ONE + instrument. TG measurements were carried out at a heating rate of 10 °C min^{-1} and in a temperature range starting from RT to 600 °C. A mass of ~ 30 mg of the investigated nanocomposite sample was introduced into the TG alumina pan. The TG measurements were done under N_2 atmosphere with a flow rate of 60 mL min^{-1}.

Results and discussion

The XRD pattern for the synthesized TiO_2 is shown in Fig. 2. The obtained pattern refers to the formation of TiO_2 anatase in good agreement with the standard data for the pure anatase TiO_2 tetragonal phase (JCPDS card no. 71–1166) without any contribution from other phases. The Miller indices (hkl) for the obtained reflection peaks are shown in Fig. 2. The two strongest peaks that are recorded at 2θ of 25.41° and 48.03° that is confirming the formation of the TiO_2 anatase structure as reported by [25, 26]. The

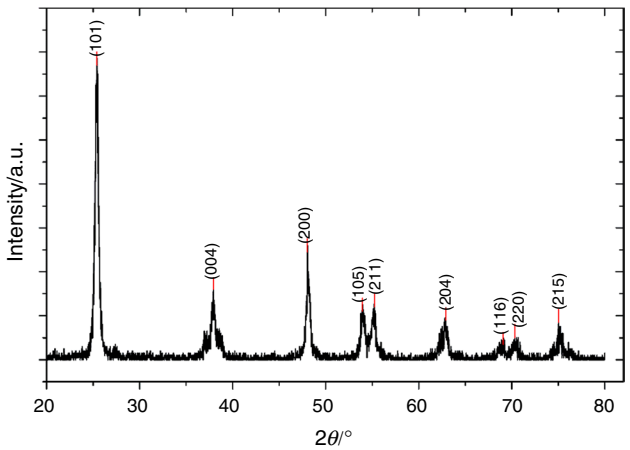

Fig. 2 XRD pattern of the synthesized TiO_2 NPs

Table 1 Thermal characteristic quantities which obtained from DSC and TG measurements as a function of mass percentage ratio betweenTiO_2 NPs and PW

Sample	TiO_2:PW/ mass%	T_m/°C	LH/Jg^{-1}	LHR/Jg^{-1} s^{-1}	$T_{5\%}$/°C	$T_{50\%}$/°C	T_f/°C	T_p/°C
P	0	60.80	165.6 ± 2.1	1.43	263.9	358.8	396.2	378. 1
P/0.05T	0.05	60.97	191.4 ± 1.7	2.88	277.5	367	418.1	385.8
P/0.1T	0.1	61.45	190.2 ± 2.4	2.83	265.3	364.8	413.4	385.8
P/0.15T	0.15	57.90	169.1 ± 2.0	2.09	284.7	374.7	419.9	395.4
P/0.2T	0.2	63.33	180.6 ± 2.1	3.35	285.6	374.4	420	396.4
P/0.25 T	0.25	62.84	184.1 ± 1.2	2.95	281.7	372.6	410.1	388
P/0.3 T	0.3	60.84	200.7 ± 2.7	2.47	246.9	349.7	388. 7	366
P/0.5 T	0.5	58.97	184.0 ± 1.9	2.40	262	363.3	418. 1	379.6

peak intensity illustrated in the XRD pattern declares that the TiO_2 NPs are crystalline with very small crystallites due to the broadening in the diffraction peaks. The crystallite size (D) could be estimated using the Debye–Scherrer formula [27]:

$$D = \frac{0.94\lambda}{\beta \cos\theta} \tag{1}$$

where λ is the wavelength of the X-ray ($\lambda = 0.15406$ nm), β is the FWHM (full width at half maximum in radians), and θ is the diffraction angle. The obtained average value of D for the three most preferred orientation peaks, (101), (004) and (200), was found to be 22.75 nm. In contrast to the Debye–Scherrer method, the Williamson–Hall (W–H) method considers the effect of the induced strain on the peak broadening. Consequently, the W–H method can be used for the estimation of the value of D without the influence of strain. In this respect, a W–H plot can be achieved using the following equation [28]:

$$\beta \cos\theta = 4\varepsilon \sin\theta + \frac{K\lambda}{D} \tag{2}$$

where K is shape factor (0.94) and ε is the induced strain in powders due to crystal imperfection and/or distortion. Figure 3 shows the W–H plot between $4\varepsilon \sin\theta$ versus $\beta \cos\theta$ for all the obtained diffraction peaks.

Using the linear regression least squares fitting, the slope of the obtained straight line is equal to $\varepsilon = -0.004$. However, the average value of D could be calculated from the y intercept of the liner fit and Eq. (2) and it was found to be 12.75 nm. Moreover, the lattice constants a and c were estimated by applying XRD data for tetragonal crystal configuration and were found to be 0.377 nm and 0.948 nm, respectively. The obtained values of the lattice constants for the investigated TiO_2 NPs are in good agreement with those commonly obtained for TiO_2 as in the standard data in card no JCPDS file no. 71–1166 [29].

The morphology of the synthesized TiO_2 NPs and the fabricated PW/TiO_2 NCs was examined by FE-SEM. Figure 4 illustrates the FE-SEM micrographs for the synthesized TiO_2 NPs. As shown in Fig. 4, the particles have a well-defined spherical shape with a diameter in the nanometer range. The obtained NPs have quite homogeneity in size and shape, with an agglomerated structure. Such agglomeration could be attributed to the high surface energy of the NPs. Figure 5 illustrates the micrographs of P, P/0.2T and P/0.5T NC samples. In contrast to Fig. 5a for pure PW, Fig. 5b and c reveals small bright sites that are related to the TiO_2 nanoparticle fillers throughout the PW. The obtained FE-SEM micrographs of P/0.2T and P/0.5T NC samples exhibit a reasonably good dispersion of TiO_2 NPs throughout the host PW. `Consequently, the used fabrication route for NCs offered a good interaction between TiO_2 nanoparticle and PW. However, the obtained micrographs for P/0.5T NC, Fig. 5c, have a higher density of NPs in comparison with those obtained for P/0.2T NC as seen in Fig. 5b. Obliviously, such variation is due to the different concentrations of the NPs in both NCs. Such variation could have an effect on the thermal properties of the studied NCs, as will be discussed later.

Figure 6 illustrates the DSC curves of the investigated PW/TiO_2 NCs that are obtained at a constant heat rate of 10 °C min^{-1}. The DSC curve for each NC sample is characterized by two endothermic peaks, which are assigned

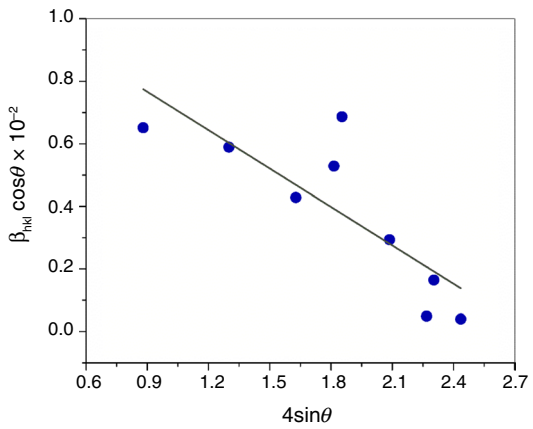

Fig. 3 Williamson–Hall plot of 4sinθ on the x-axis and βcosθ on the y-axis for the synthesized TiO_2 NPs

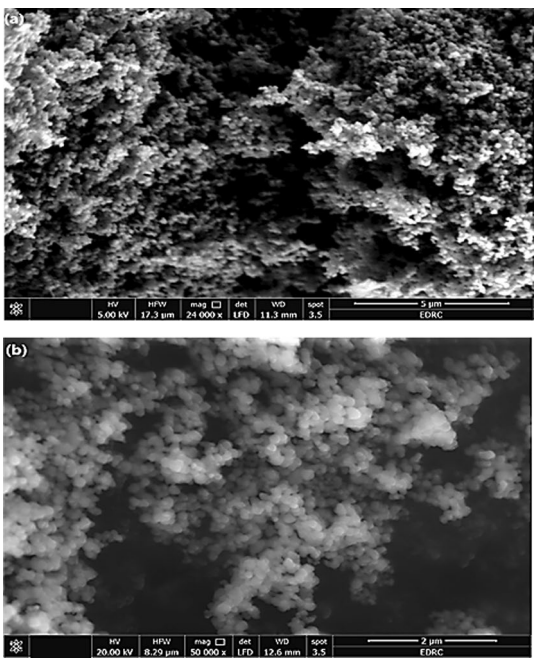

Fig. 4 FE-SEM micrographs for the synthesized TiO_2 NPs: **a** image with 24,000× magnification and 5-μm scale; **b** image with 50,000× magnification and 2-μm scale

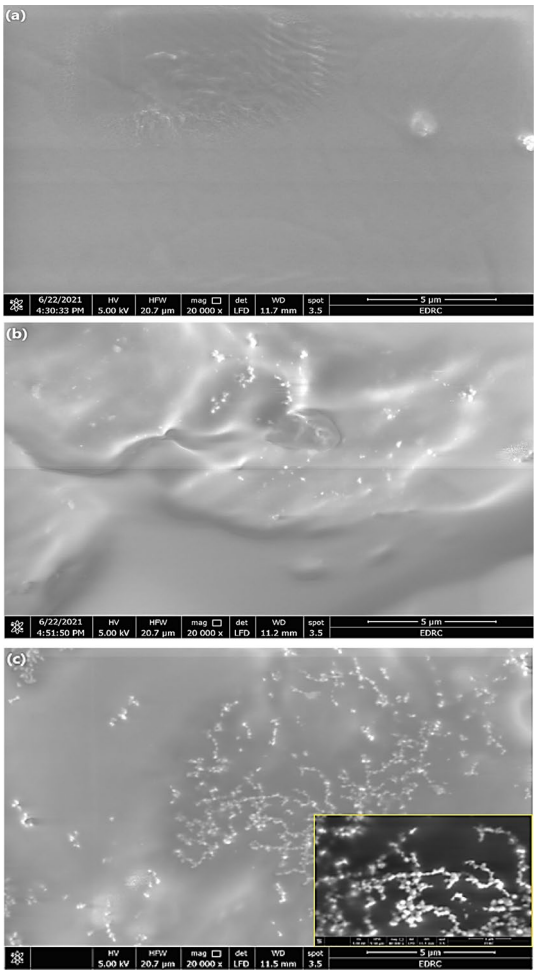

Fig. 5 FE-SEM micrographs with 20,000× magnification and 5-µm scale for NCs: **a** P; **b** P/0.2 T; **c** P/0.5 T

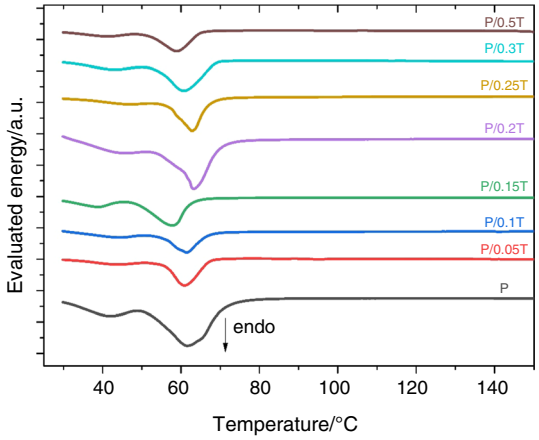

Fig. 6 DSC curves for the investigated PW/TiO_2 NCs

to the solid–solid transition followed by the solid–liquid transition. In fact, solid–solid transition occurs by changing temperature or pressure, which is the polymorphic feature in material due to transformation from a certain crystalline solid configuration into another form of crystalline solid [30]. Commonly, the crystalline solid–solid transitions are accompanied by sporadic variations in volume, enthalpy, and entropy as a result of crystal packing modifications. Such variations have small values compared to those occurring due to solid–liquid transitions.

The characteristic parameters of the solid–liquid transition (melting process) as a function of TiO_2 NP concentration were estimated and listed in Table 1. These parameters are melting temperature (T_m, temperature at maximum rate of melting), latent heat of melting (LH) and latent heat rate (LHR). The obtained values of LH exhibited that all the investigated NCs have a higher latent heat capacity than pure PW. Such a result refers to the good interaction between the high surface area of TiO_2 NPs and PW molecules throughout the investigated concentration range. Moreover, the difference in coordination geometry of NP structures related to surface defect sites enhances the latent heat capacity of NCs [31]. The highest value of the LH, 200.7 ± 2.7 Jg^{-1} was obtained for 0.3 mass% loading of TiO_2 NPs with an improvement ~ 21.2% compared to that obtained for pure PW. An improvement in the latent heat capacity of ~ 14% has been obtained for 0.7 mass% loading of TiO_2 NPs as reported by Wang et al. [18].

By dividing the obtained LH for each sample from DSC measurements by the corresponding period of melting process, the LHR values were computed. In fact, LHR refers to the amount of energy that can be stored in the material per unit time during the melting process, which gives information about the thermal-storage power of such material. According to the obtained LHR values of the investigated NCs, the highest value of LHR, 3.35 Jg^{-1} s^{-1}, was estimated for NC sample with 0.2 mass% loading of TiO_2 NPs, with an improvement ~ 134.3% than that estimated for pure PW. In this respect, Fig. 7 shows the non-monotonic variation of LH and LHR as a function of TiO_2 nanoparticle concentrations. Such a figure reveals the difference in the trend of variation for both LH and LHR with nanoparticle concentration. Namely, the NCs with high concentrations of NPs (P/0.25T, P/0.3T, and P/0. 5T) recorded higher LH values than that recorded for P/0.2T NC. This result was reversed for LHR values for these samples, which could be explained in view of the influence of viscosity variation on the natural convective heat transfer. It should be noted that the loading of NPs into PW varies the dynamic behavior of the material. Specifically, beside the increase in thermal conductivity of PCM by addition of NPs, an obvious increase in melt viscosity happens, which weakens in the heat transfer of melt via natural convection [32]. This limitation in the natural convective heat transfer, for NCs with high loading by NPs, was compensated by the significant enhancement in thermal

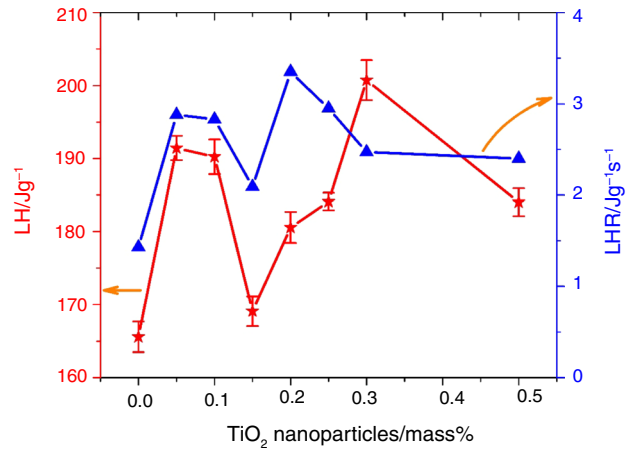

Fig. 7 The variation of LH and LHR with TiO_2 NP mass percentages

conductivity as exhibited in LHR behavior for P/0.25T, P/0.3T, and P/0.5T, as shown in Fig. 7. The obtained results showed that P/0.2T NC introduced the highest storage power value of heat for 1 g which means this sample has the highest effective heat capacity of the other investigated samples.

The thermal stability of the investigated PW/TiO_2 samples was studied using the TG technique and their derivative thermogravimetric (DTG) analysis. Figure 8 illustrates the TG curves of the pure PW sample and the other investigated PW/TiO_2 NCs. As shown in Fig. 8, all the studied samples degraded through a single step behavior. Table 1 lists the degradation characteristic temperatures obtained from TG scans depending on the mass ratio percentage (mass%) of the synthesized TiO_2 NPs. Those characteristic temperatures are: $T_{5\%}$ (the temperature of degradation at which 5% of the degradation happens), $T_{50\%}$ (the temperature at which 50% of the degradation happens), T_f (the final temperature at which the degradation process ends), and T_p (peak temperature at the maximum rate of the degradation process), which are obtained from Fig. 9 that shows the DTG versus temperature for all the investigated samples. The dependence of the characteristic temperatures on TiO_2 NPs concentration exhibited a non-monotonic behavior. Specifically, the addition of TiO_2 NPs up to 0.25 mass% improves the thermal stability of the NCs in comparison with a pure PW sample. This result is clearly noticeable due to the high recorded values of all degradation characteristic temperatures for NCs up to 0.25 mass% of TiO_2 compared with those obtained for a pure PW sample. However, the samples with high NP concentrations, P/0.3T and P/0.5T, have lower thermal stability and lower degradation temperatures than the pure PW sample. The enhancement in thermal stability of organic materials is commonly obtained by introducing inorganic NPs, especially in cases of good dispersion of NPs throughout the host material [33]. Indeed, the inorganic NPs with good thermal conductivity and heat capacity, such as TiO_2, are acting as good heat sinks limit the fast degradation of the host organic materials [34]. It is worth noting that, by introducing 0.2 mass% TiO_2 NPs into PW, P/0.2T NC, T_p and T_f were delayed in comparison with the pure sample by 18.3 °C and 23.8 °C, respectively. As an illustration of the typical degradation temperatures, Fig. 10 shows the range in T_p values of the examined samples. The improvement in thermal stability of the investigated NCs disappeared for the high concentrations of TiO_2 NPs, P/0.3T and P/0.5T NCs, which could be attributed to NPs' agglomeration above the optimum value of loading. So, the degradation process of such samples became fast due the probable transformation from nanostructure feature to microstructure feature due to the agglomeration of the NPs.

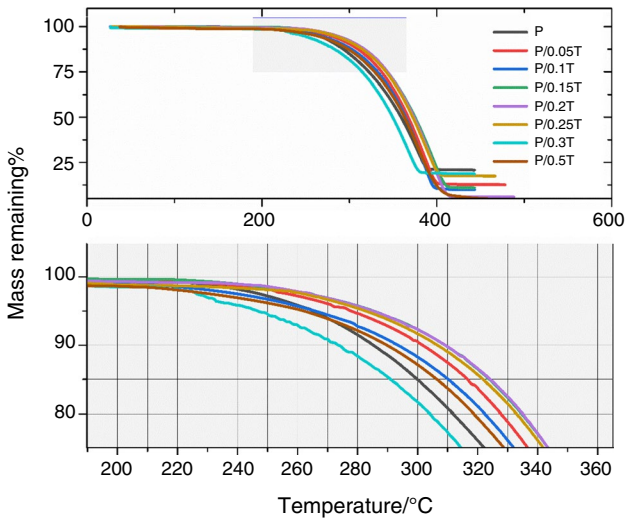

Fig. 8 TG curves for the pure PW sample and the other studied PW/TiO_2 NCs

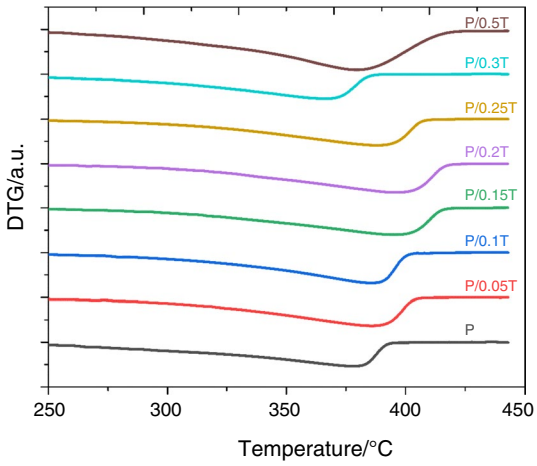

Fig. 9 DTG versus temperature curves for the pure PW sample and the other studied PW/TiO_2 NCs

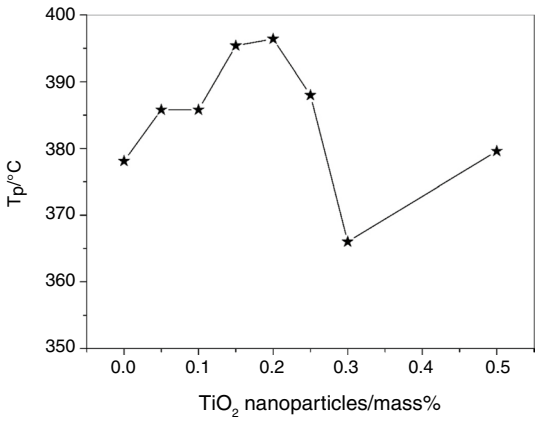

Fig. 10 Variation of Tp values as a function of TiO_2 NP mass percentages

Conclusions

PW NCs loaded by TiO_2 NPs with various concentrations in a small range up to 0.5 mass% have been successfully fabricated. The used TiO_2 NPs were synthesized using the simple hydrolysis route of TTIP. The acquired XRD data have revealed that the synthesized TiO_2 NPs are in a pure anatase tetragonal phase. FE-SEM micrographs were used to achieve and confirm the excellent dispersion of TiO_2 NPs into PW, demonstrating a positive interaction between the two materials. With the aid of non-isothermal DSC and TG measurements, the impact of TiO_2 NP addition on the thermal characteristics of PW was examined. The inclusion of TiO_2 NPs resulted in a notable improvement in PW's thermal performance. In this respect, the improvement in latent heat capacity was reached at ~ 21.2% for 0.3 mass% loading of TiO_2 NPs. However, the thermal LHR showed a significant increase, reaching ~ 134.3% for P/0.2T in comparison with PW. Such a significant enhancement in LHR by the introduction TiO_2 NPs gives a promising indication of the capability of the examined PW NCs in thermal storage applications. Nevertheless, LHR values decreased for concentrations higher than 0.2 mass%, which could be attributed to limitations in the natural convective heat transfer as a result of the increase in melt viscosity. The TG analysis of the PW/ TiO_2 NCs showed a positive impact on delaying the degradation process with the addition of TiO_2 NPs up to 0.25 mass%. Such a result confirmed the high surface area of non-degradable NPs throughout PW. The thermal properties investigation of PW/TiO_2 NCs concluded the possibility of using such NCs as efficient and thermally stable PCMs. However, it is advised that future work investigate the thermal characteristics of such NCs over the course of the full heating–cooling cycle(s) and optimize the dispersion of NPs within the PW.

Funding Open access funding provided by The Science, Technology & Innovation Funding Authority (STDF) in cooperation with The Egyptian Knowledge Bank (EKB).

Declarations

Conflict of interest The author(s) declared no potential conflicts of interest with respect to the research, authorship, and/or publication of this article.

Open Access This article is licensed under a Creative Commons Attribution 4.0 International License, which permits use, sharing, adaptation, distribution and reproduction in any medium or format, as long as you give appropriate credit to the original author(s) and the source, provide a link to the Creative Commons licence, and indicate if changes were made. The images or other third party material in this article are included in the article's Creative Commons licence, unless indicated otherwise in a credit line to the material. If material is not included in the article's Creative Commons licence and your intended use is not permitted by statutory regulation or exceeds the permitted use, you will need to obtain permission directly from the copyright holder. To view a copy of this licence, visit http://creativecommons.org/licenses/by/4.0/.

References

1. Pielichowska K, Pielichowski K. Phase change materials for thermal energy storage. Prog Mater Sci. 2014;65:67–123. https://doi.org/10.1016/j.pmatsci.2014.03.005.
2. Teggar M, Arıcı M, Mert MS, Ajarostaghi SSM, Niyas H, Tunçbilek E, Ismail KAR, Younsi Z, Benhouia AT, Mezaache EH. A comprehensive review of micro/nano enhanced phase change materials. J Therm Anal Calorim. 2022;147:3989–4016. https://doi.org/10.1007/s10973-021-10808-0.
3. Tan N, Ning YH, Hu P, et al. Silica-confined composite form-stable phase change materials: a review. J Therm Anal Calorim. 2022;147:7077–97. https://doi.org/10.1007/s10973-021-11037-1.
4. Kürklü A, Özmerzi A, Bilgin S. Thermal performance of a water-phase change material solar collector. Renew Energy. 2002;26:391–9. https://doi.org/10.1016/S0960-1481(01)00130-6.
5. Zalba B, Marín JM, Cabeza LF, Mehling H. Review on thermal energy storage with phase change: materials, heat transfer analysis and applications. Appl Therm Eng. 2003;23:251–83. https://doi.org/10.1016/S1359-4311(02)00192-8.
6. Sokar MS, Mansour SA, Ali AA, Elnekiety MH. Investigation of paraffin wax with ZnO nanorods for performance enhancement of solar thermal energy storage. Mansoura Eng J. 2020;45:19–28. https://doi.org/10.21608/bfemu.2020.111571.
7. Ho CJ, Gao JY. Preparation and thermophysical properties of nanoparticle-in-paraffin emulsion as phase change material. Int Commun Heat Mass Transfer. 2009;36:467–70. https://doi.org/10.1016/j.icheatmasstransfer.2009.01.015.
8. Tony MA, Mansour SA. Sunlight-driven organic phase change material-embedded nanofiller for latent heat solar energy storage. Int J Environ Sci Technol. 2020;17:709–20. https://doi.org/10.1007/s13762-019-02507-z.
9. Karunamurthya K, Murugumohankumarb K. Use of Cuo nanomaterial for the improvement of thermal conductivity and performance of low temperature energy storage system of solar pond. Dig J Nanomater Biostruct. 2012;7:1833–41.
10. Chinnaiyan K, Prakash D. Review on phase change materials with nanoparticle in engineering applications. J Eng Sci Technol Rev. 2016;9:26–36. https://doi.org/10.25103/jestr.094.05.

11. Bafakeeh OT, Shiba MS, Elshalakany AB, et al. Effect of dispersion hybrid structural properties of MWCNTs and Al_2O_3 on microstructural and thermal characteristics of PCMs for thermal energy storage in solar water desalination. J Therm Anal Calorim. 2023;148:4087–104. https://doi.org/10.1007/s10973-023-11973-0.
12. Han Z, Fina A. Thermal conductivity of carbon nanotubes and their polymer nanocomposites: a review. Prog Polym Sci. 2011;36(7):914–44. https://doi.org/10.1016/j.progpolymsci.2010.11.004.
13. Aslfattahi N, Saidur R, Arifutzzaman A, et al. Improved thermophysical properties and energy efficiency of hybrid PCM/graphene–silver nanocomposite in a hybrid CPV/thermal solar system. J Therm Anal Calorim. 2022;147:1125–42. https://doi.org/10.1007/s10973-020-10390-x.
14. Ranjbar S, Masoumi H, Khoshkhoo RH, et al. Experimental investigation of stability and thermal conductivity of phase change materials containing pristine and functionalized multi-walled carbon nanotubes. J Therm Anal Calorim. 2020;140:2505–18. https://doi.org/10.1007/s10973-019-09005-x.
15. Chaichan MT, Kazem HA, Alamiery AA, Isahak WNRW, Kadhum AAH, Takriff MS. Adding nano-TiO_2 to water and paraffin to enhance total efficiency of a photovoltaic thermal PV/T system subjected to harsh weathers. Nanomaterials (Basel). 2022;30(12):2266. https://doi.org/10.3390/nano12132266.
16. Nabhan BJ. Using nanoparticles for enhance thermal conductivity of latent heat thermal energy storage. J Eng. 2015;21:37–51.
17. Teng TP, Yu CC. Characteristics of phase-change materials containing oxide nano-additives for thermal storage. Nanoscale Res Lett. 2012;7:611–611. https://doi.org/10.1186/1556-276X-7-611.
18. Wang J, Xie H, Guo Z, Guan L, Li Y. Improved thermal properties of paraffin wax by the addition of TiO_2 nanoparticles. Appl Therm Eng. 2014;73(2):1541–7. https://doi.org/10.1016/j.applthermaleng.2014.05.078.
19. Said Z, Sundar LS, Tiwari AK, Ali HM, Sheikholeslami M, Bellos E, Babar H. Recent advances on the fundamental physical phenomena behind stability, dynamic motion, thermophysical properties, heat transport, applications, and challenges of nanofluids. Phys Rep. 2022;946:1–94. https://doi.org/10.1016/j.physrep.2021.07.002.
20. Zhang H, Banfield JF. Thermodynamic analysis of phase stability of nanocrystalline titania. J Mater Chem. 1998;8(9):2073–6. https://doi.org/10.1039/A802619J.
21. Cabaleiro D, Nimo J, Pastoriza-Gallego M, Piñeiro M, Legido J, Lugo L. Thermal conductivity of dry anatase and rutile nano-powders and ethylene and propylene glycol-based TiO_2 nanofluids. J Chem Thermodyn. 2015;83:67–76. https://doi.org/10.1016/j.jct.2014.12.001.
22. Mitra D, Howli P, Das BK, Das NS, Chattopadhyay P, Chattopadhyay KK. Size and phase dependent thermal conductivity of TiO_2-water nanofluid with theoretical insight. J Mol Liq. 2020;302:11249. https://doi.org/10.1016/j.molliq.2020.112499.
23. Mansour SA. Non-isothermal crystallization kinetics of nano-sized amorphous TiO_2 prepared by facile sonochemical hydrolysis route. Ceram Int. 2019;45:2893–8. https://doi.org/10.1016/j.ceramint.2018.07.273.
24. Alkallas FH, Elshokrofy KM, Mansour SA. Structural and diffuse reflectance characterization of cobalt-doped titanium dioxide nanostructured powder prepared via facile sonochemical hydrolysis technique. Nanomater Nanotechnol. 2019;9:1847980419847806. https://doi.org/10.1177/1847980419847806.
25. Mansour SA, Farha AF, Kotkata MF. Sol–gel synthesized co-doped anatase TiO_2 nanoparticles: structural, optical, and magnetic characterization. J Inorg Organomet Polym Mater. 2019;29:1375–82. https://doi.org/10.1007/s10904-019-01102-6.
26. Thamaphat K, Limsuwan P, Ngotawornchai B. Phase characterization of TiO_2 powder by XRD and TEM\n. Nat Sci. 2008;42:357–61.
27. Langford JI, Wilson AJC. Scherrer after sixty years: a survey and some new results in the determination of crystallite size. J Appl Crystallogr. 1978;11:102–13. https://doi.org/10.1107/S0021889878012844.
28. Mote V, Purushotham Y, Dole B. Williamson–Hall analysis in estimation of lattice strain in nanometer-sized ZnO particles. J Theor Appl Phys. 2012;6:6. https://doi.org/10.1186/2251-7235-6-6.
29. Alkallas FH, Al-Rebdi TA, Mansour SA. Structural and diffuse reflectance investigation of dysprosium-doped TiO_2 nanopowder synthesized by sonochemical hydrolysis technique. Physica B Condens Matter. 2021;603:412664. https://doi.org/10.1016/j.physb.2020.412664.
30. Cheng SZD. Thermodynamics and kinetics of phase transitions. In: Cheng SZD, editor. Phase transitions in polymers. Amsterdam: Elsevier; 2008. p. 17–59. https://doi.org/10.1016/B978-0-444-51911-5.00002-5.
31. Sahan N, Paksoy HO. Thermal enhancement of paraffin as a phase change material with nanomagnetite. Sol Energy Mater Sol Cells. 2014;126:56–61. https://doi.org/10.1016/j.solmat.2014.03.018.
32. Bondareva NS, Sheremet MA. Effect of nano-sized heat transfer enhancers on PCM-based heat sink performance at various heat loads. Nanomaterials. 2020;10:17. https://doi.org/10.3390/nano10010017.
33. Farha A, Naim A, Mansour S. Thermal degradation of polystyrene (PS) nanocomposites loaded with sol gel-synthesized ZnO nanorods. Polymers. 2020;12:1935. https://doi.org/10.3390/polym12091935.
34. Manoj KP, Mylsamy K, Saravanakumar PT, Anandkumar R, Pranav A. Experimental Study on thermal properties of nano-TiO_2 embedded paraffin (NEP) for thermal energy storage applications. Mater Today Proc. 2020;22:2153–9. https://doi.org/10.1016/j.matpr.2020.03.282.

Publisher's Note Springer Nature remains neutral with regard to jurisdictional claims in published maps and institutional affiliations.